

Predictions of Quark-Gluon String Model for pp at LHC

A.B. Kaidalov¹ and M.G. Poghosyan²

¹Institute of Theoretical and Experimental Physics, 117259 Moscow, Russia

²Università di Torino/INFN, 10125 Torino, Italy

Abstract

Soft multiparticle production processes in hadronic collisions are considered in the framework of the Quark-Gluon Strings Model and the model predictions are compared with data from $Spp\bar{S}$ and Tevatron. Predictions for LHC energies are given.

1 Introduction

In hadronic collisions soft interactions are dominant. These are characterized by large distances ($r \sim 1/\Lambda_{QCD}$) and the pQCD cannot be used for their study.

Regge-pole theory is the main method for description of high-energy soft processes and the Pomeron is the main object of this approach, which is associated with cylinder-type diagrams of $1/N$ expansion in QCD. $1/N$ expansion is a dynamical expansion and the speed of convergence depends on the kinematical region of studying process. At very high energies many terms of the expansion (multi-pomeron exchanges) should be taken into account.

The models of Quark-Gluon Strings (QGSM) [1] and Dual-Parton Model (DPM) [2], are based on nonperturbative notions, combining $1/N$ expansion in QCD with Regge theory and using parton structure of hadrons. Here we concentrate on QGSM, which has been successfully applied to many different problems of strong interactions: hadronic mass spectrum [3], widths of resonances [4], relations between the total cross-sections, residues of Regge poles [4], behavior of hadronic form factors [5], baryon number transfer [6], and multiparticle production at high energies [1, 6, 7, 8].

In this paper we briefly describe QGSM, compare its predictions with $Spp\bar{S}$ and Tevatron data on charged particles pseudorapidity and multiplicity distributions and give predictions for LHC.

2 QGSM

In QGSM the production of a particle is defined through production of showers and each shower corresponds to the cut-pomeron pole contribution in the elastic scattering amplitude. For hadron-hadron collisions the cross-section of n cut-pomeron exchange (among arbitrary number of uncut pomerons) is calculated in “quasi-eikonal” approximation and has the following form [9]:

$$\sigma_n(\xi) = 4\pi \frac{\lambda}{nC} \left[1 - \exp\{-z\} \sum_{l=0}^{n-1} \frac{z^l}{l!} \right]. \quad (1)$$

Where $z = C\gamma/\lambda \exp\{\Delta\xi\}$, $\lambda = R^2 + \alpha'_P \xi$, and $\xi = \ln(s/s_0)$. The values of parameters γ , λ , R^2 and α'_P which characterize the residue and the trajectory of the pomeron are found from fit to data on pp and $p\bar{p}$ total interaction and elastic scattering cross-section in Ref. [10]: $\gamma = 2.14 \text{ GeV}^{-2}$, $R^2 = 3.3 \text{ GeV}^{-2}$, $\Delta = 0.12$, $\alpha'_P = 0.22 \text{ GeV}^{-2}$. The parameter C , which is related to small-mass diffraction dissociation of incoming hadrons during the rescattering is equal to 1.5 [11]. The sum of σ_n ($n = 1, 2, 3, \dots$) defines the cross-section of non-diffractive interaction.

The association of the pomeron with cylinder-type diagrams leads to the fact that in a single cut-pomeron diagram there are two chains of particles (strings). Analogously, in case of n cut-pomerons there are $2n$ chains. Inclusive distribution in rapidities and multiplicity distribution of particles for non-diffractive events can be expressed in terms of rapidity distributions, $f_n(\xi, y)$, and multiplicity distribution, $W_n(\xi, N)$, for $2n$ -chains [1]:

$$\frac{d\sigma(\xi)}{dy} = \sum_n \sigma_n(\xi) f_n(\xi, y), \quad (2)$$

$$\sigma(\xi, N) = \sum_n \sigma_n(\xi) W_n(\xi, N).$$

In order to calculate the distribution of hadrons produced during the fragmentation of the strings one should

take into account that the hadron can be produced in each of the $2n$ -chains and the (di-)quarks, which stretch the strings, carry only a fraction of energy of the incoming protons. In these terms, the inclusive spectra can be written as convolutions of the probabilities to find a string with certain rapidity length and the fragmentation functions, which defines the distribution of hadrons in the string breaking process. For pp collisions the function $f_n(\xi, y)$ is written as follows [1]:

$$f_n^h(\xi, y) = a^h \left[F_{qval}^{h(n)}(x_+) F_{qq}^{h(n)}(x_-) + F_{qq}^{h(n)}(x_+) F_{qval}^{h(n)}(x_-) + 2(n-1) F_{qsea}^{h(n)}(x_+) F_{qsea}^{h(n)}(x_-) \right],$$

where $x_{\pm} = (1/2)[\sqrt{x_T^2 + x^2} \pm x]$, $x_T = 2m_T/\sqrt{s}$ and x is the Feynman- x of produced hadron h . a^h is the density of hadrons h produced at mid-rapidity in a single chain and its value is determined from experimental data. In fact these are the only free parameters in the model that are fixed from fit to data. In articles [1],[6] and [7] the following values are found for them: $a^{\pi} = 0.44$, $a^K = 0.055$, $a^p = 0.07$. The first two terms in Eq. (3) correspond to the chains, which connect “valence” quarks and di-quarks¹, and the last term corresponds to chains connected to the sea quarks-antiquarks. Here we do not consider the contribution of sea di-quarks and anti-diquarks, their contribution is important in the spectra of anti-baryons produced in the forward region [12]. The functions $F_i^{h(n)}(x)$ being a convolution of the structure $\psi(x)$, and fragmentation $G(x)$ functions are written as follows:

$$\begin{aligned} F_{qval}^{h(n)}(x_{\pm}) &= \frac{2}{3} \int_{x_{\pm}}^1 dx \psi_{uval}(n, x) G_u^h\left(\frac{x_{\pm}}{x}\right) \\ &\quad + \frac{1}{3} \int_{x_{\pm}}^1 dx \psi_{dval}(n, x) G_d^h\left(\frac{x_{\pm}}{x}\right), \\ F_{qq}^{h(n)}(x_{\pm}) &= \frac{2}{3} \int_{x_{\pm}}^1 dx \psi_{ud}(n, x) G_{ud}^h\left(\frac{x_{\pm}}{x}\right) \\ &\quad + \frac{1}{3} \int_{x_{\pm}}^1 dx \psi_{uu}(n, x) G_{uu}^h\left(\frac{x_{\pm}}{x}\right), \\ F_{qsea}^{h(n)}(x_{\pm}) &= \frac{1}{2+\delta} \left[\int_{x_{\pm}}^1 dx \psi_{usea}(n, x) G_u^h\left(\frac{x_{\pm}}{x}\right) \right. \\ &\quad \left. + \int_{x_{\pm}}^1 dx \psi_{dsea}(n, x) G_d^h\left(\frac{x_{\pm}}{x}\right) + \right. \end{aligned}$$

¹In case of $p\bar{p}$ collisions they must be replaced by $F_{qval}^{h(n)}(x_+) F_{\bar{q}val}^{h(n)}(x_-) + F_{qq}^{h(n)}(x_+) F_{\bar{q}\bar{q}}^{h(n)}(x_-)$. This change is in order to have white objects required by QCD.

$$\delta \int_{x_{\pm}}^1 dx \psi_{ssea}(n, x) G_s^h\left(\frac{x_{\pm}}{x}\right) \Bigg].$$

Where δ is the strangeness suppression parameter ($\delta \approx 1/3$).

In the model, the structure and fragmentation functions are determined by the corresponding Regge asymptotic behaviors in the regions $x \rightarrow 0$ and $x \rightarrow 1$ and for the full range of x an interpolation is done.

The structure functions of a proton are parameterized as follows [6, 7]:

$$\begin{aligned} \psi_{d_v}(x, n) &= \psi_{d_s}(x, n) = C_d x^{-\alpha_R} (1-x)^{\alpha_R-2\alpha_B+n}, \\ \psi_{u_v}(x, n) &= \psi_{d_s}(x, n) = C_u x^{-\alpha_R} (1-x)^{\alpha_R-2\alpha_B+n-1}, \\ \psi_{ud}(x, n) &= C_{ud} x^{\alpha_R-2\alpha_B} (1-x)^{\alpha_R+n-1}, \\ \psi_{uu}(x, n) &= C_{uu} x^{\alpha_R-2\alpha_B+1} (1-x)^{\alpha_R+n-1}, \\ \psi_s(x, n) &= C_s x^{-\alpha_R} (1-x)^{2(\alpha_R-\alpha_B)-\alpha_{\phi}+n-1}. \end{aligned}$$

Where $\alpha_R=0.5$, $\alpha_B=-0.5$. C_i are determined from normalization condition:

$$\int_0^1 \psi_i(x, n) dx = 1.$$

General technique of constructing fragmentation functions is presented in Ref. [13]. For instance, for fragmenting to a pion the parameterizations are (see [1] and [13]):

$$\begin{aligned} G_d^{\pi^+}(z) &= G_u^{\pi^-}(z) = (1-z)^{2-3\alpha_R+\lambda}, \\ G_u^{\pi^+}(z) &= G_d^{\pi^-}(z) = (1-z)^{-\alpha_R+\lambda}, \\ G_s^{\pi^+}(z) &= G_s^{\pi^-}(z) = (1-z)^{1-\alpha_R+\lambda}, \\ G_{ud}^{\pi^+}(z) &= G_{ud}^{\pi^-}(z) = (1-z)^{\alpha_R+\lambda-2\alpha_B} (1-z+z^2/2), \\ G_{uu}^{\pi^+}(z) &= (1-z)^{\alpha_R+\lambda-2\alpha_B}, \\ G_{uu}^{\pi^-}(z) &= (1-z)^{\alpha_R+\lambda-2\alpha_B+1}. \end{aligned}$$

We do not list fragmentation functions for kaons and (anti-)protons, they are taken from Ref. [6, 7].

In hadronic interactions diffractive processes play an important role. Densities of produced particles in these processes are small, especially in the central rapidity region, but their cross-section is not negligible with respect to non-diffractive cross-section and they must be taken into account in calculations of characteristics of secondary particles. In Ref. [14] single- and double-diffractive processes are described in terms of dressed triple-reggeon and loop diagrams. For instance, for calculating the rapidity distribution of particles produced

in soft single-diffractive events the first equation in (2) must be replaced by (see [8]):

$$\frac{d\sigma}{dy} = \sum_n \int d\zeta \frac{d\sigma_n}{d\zeta} f_n(\zeta, y). \quad (4)$$

Here $d\sigma/d\zeta$ is the derivative of single-diffraction dissociation cross-section, $\zeta = M^2/s$, and M is the mass of the diffracted system.

The model does not contain “odderon”-type singularities with negative signature, which could lead to a difference of pp and $p\bar{p}$ scattering, so at energies $\sqrt{s} \geq 100$ GeV all characteristics of pp and $p\bar{p}$ interactions coincide.

3 Numerical results

QGSM has been used successfully to describe data on secondary hadron inclusive cross-sections integrated over transverse momentum, such as rapidity and multiplicity distributions, ratios of particles and it explains many characteristic features of hadron-hadron soft interactions. But for calculating pseudorapidity distribution from Eq. (2) or (4) we must know mean transverse momentum of particles.

Though the model does not give predictions on p_t –dependence, some conclusions can be obtained from its basics (or from Gribov’s Reggeon calculus in general). As it is already mentioned, the multi-particle production is described in terms of cut-pomeron diagrams. On the other hand, using Eq. (1) it is easy to see that the mean number of cut-pomerons increases with energy $\sim s^\Delta$. Average transverse momenta of produced particles increase with the number of chains: $p_t \sim \sqrt{N}$. So, we expect at LHC energies to have mean transverse momentum of produced particles higher then the one measured at ISR energies. Analogously, the selection of events with high multiplicity results in an increase of cut-pomerons number and to an increase of $\langle p_t \rangle \sim \sqrt{N}$. This dependence is observed experimentally by UA1 and CDF collaborations ([15] and [16]). Only in cases of [16] the values of measurements are published and in Fig. 3 we compare our expected dependence with these data. The fit result is:

$$p_t = (0.62973 \pm 0.00084) + (0.0717848 \pm 0.00024) \sqrt{N_{ch}}. \quad (5)$$

In order to convert rapidity to pseudorapidity distributions we used experimentally measured $\langle p_t \rangle$ for different types of particles (here we assume that the sample of secondary charged particles consists from π^+ , K^+ and

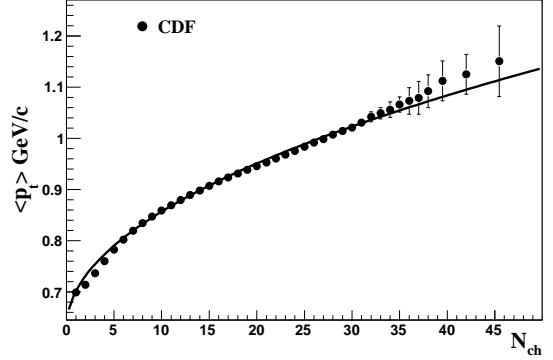


Figure 1: Comparison of phenomenologically expected dependence of mean transfers momentum of secondary particles on charged particles multiplicity with experimental data from CDF [16].

protons, and their anti-particles). In Ref. [8] we have parameterized $\langle p_t \rangle$ as a function of \sqrt{s} for charged pions, kaons and anti-protons, and found a successful fit to the data from ISR to Tevatron energies with the second-order polynomial function of $\ln(s)$. Fit result is [8]:

$$\begin{aligned} \langle p_t^\pi \rangle &= 0.34 - 0.002 \ln s + 0.00035 \ln^2 s, \\ \langle p_t^K \rangle &= 0.55 - 0.031 \ln s + 0.001 \ln^2 s, \\ \langle p_t^p \rangle &= 0.65 - 0.045 \ln s + 0.0036 \ln^2 s. \end{aligned} \quad (6)$$

In the following for each energy and for each particle type we calculate p_t using (6).

In Fig. 2 we give description of $Spp\bar{S}$ and Tevatron data on charged particles pseudorapidity distributions in $p\bar{p}$ non-single diffractive (NSD) events and give a prediction for $\sqrt{s} = 14$ TeV.

Energy dependence of charged particles pseudorapidity density for $Spp\bar{S}$ NSD events in the central rapidity region is compared with data in Fig. 3. In the supercritical Pomeron ($\Delta > 0$) theory with account of “non-enhanced” diagrams (without interaction between Pomerons), which we consider now, inclusive cross-sections $d\sigma_c/dy$ at very high energies and at $y \simeq 0$ increase with energy as $(s/s_0)^\Delta$ (see the first article in Ref. [1] for more details). This means, in particular, that an energy dependence of inclusive spectra in the central rapidity region gives more reliable information on the value of Δ , than an energy dependence of σ_{tot} , where pomeron cuts strongly modify energy dependence compared to the pole diagram. An integral over ra-

Table 1: Predictions for LHC on mean number of charged particles in two pseudorapidity bins and in full phase-space .

\sqrt{s} TeV	$N^{NSD}(\eta < 1)$	$N^{Inel}(\eta < 1)$	$N^{NSD}(\eta < 2.5)$	$N^{Inel}(\eta < 2.5)$	N^{NSD}	N^{Inel}
0.9	7.1	6.3	18	16	35.8	31.4
7	10.1	8.9	25.7	22.6	64.9	56.3
10	10.7	9.4	27.1	23.8	71.3	61.7
14	11.2	9.8	28.5	25	77.4	67

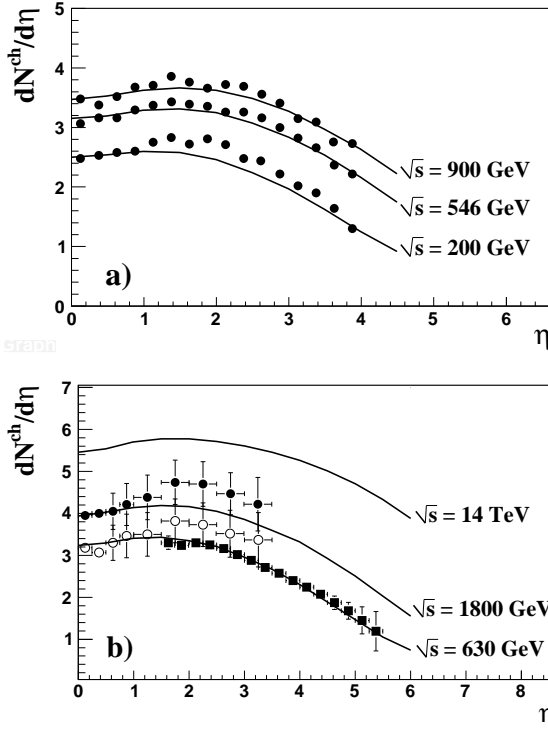


Figure 2: Comparison of model's prediction with data on charged particles pseudorapidity distribution in NSD events and prediction for LHC: a) description of UA5 data [17], b) description of CDF and P238 data (circles and squares, respectively) [18].

pidity density gives charged particles mean multiplicity $\langle N_{ch} \rangle$. In Tables 1 and 2 we list QGSM predictions on pseudorapidity density at mid-rapidity and mean number of charged particles for pp interactions at various energies of LHC. Charged particles mean multiplicity is calculated for $|\eta| < 1$ and $|\eta| < 2.5$ pseudorapidity bins, corresponding to ALICE [20] and ATLAS/CMS [21] detectors central barrel acceptances, respectively, and for full phase-space.

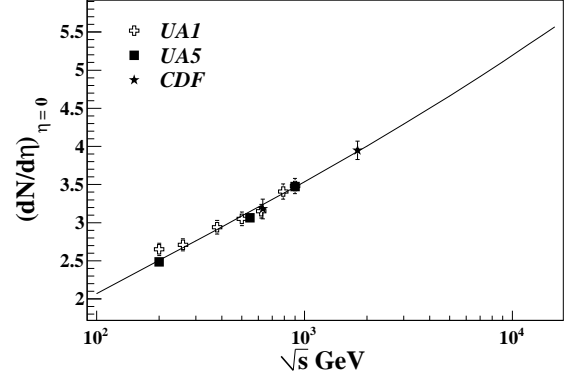


Figure 3: Energy dependence of charged particles pseudorapidity density at $\eta = 0$ for NSD events. Data are taken from [17, 18, 19].

Table 2: Predictions for LHC on charged particles pseudorapidity density at mid-rapidity.

\sqrt{s} TeV	$(dN^{NSD}/d\eta)_{\eta=0}$	$(dN^{Inel}/d\eta)_{\eta=0}$
0.9	3.5	3.
7	4.9	4.2
10	5.2	4.5
14	5.5	4.7

The multiplicity distribution in the model is given according to Eq (2) by a sum of n cut-pomerons contributions and it is assumed Poisson-like form for each contributor. In this scheme, the KNO scaling [22] is approximately valid up to ISR energies ($\sqrt{s} < 100$ GeV, where the Poissonian distributions for a different number n of cut-pomerons significantly overlap) and must be definitely violated at higher energies [23], as confirmed by measurements done at $S\bar{p}p$ S and Tevatron. In Fig. 4 we give a description of UA5 data [24] on charged particles multiplicity distribution at $\sqrt{s} = 900$ GeV and for various pseudorapidity intervals. In Fig. 5 predic-

tions for $\sqrt{s} = 14$ TeV for the full phase-space and for two pseudorapidity bins (corresponding to ALICE and ATLAS/CMS detectors central barrel acceptances) are given.

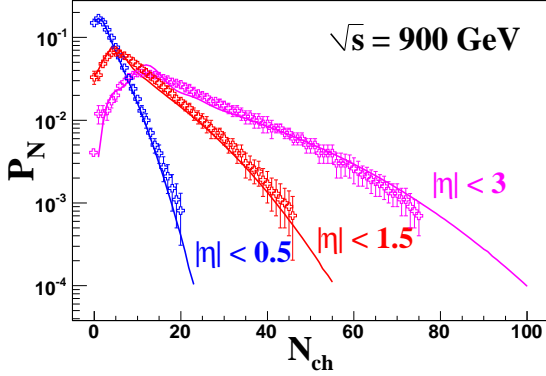


Figure 4: Comparison of model predictions with UA5 data on charged particles multiplicity distribution in NSD events at $\sqrt{s} = 900$ GeV.

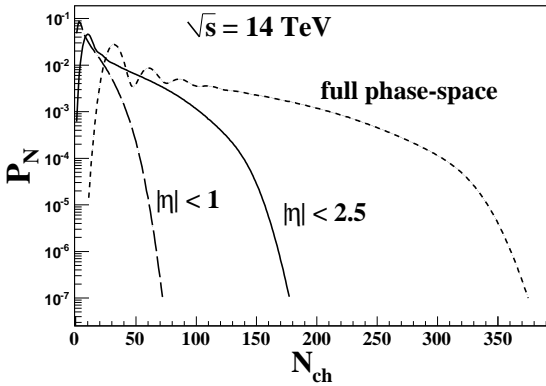


Figure 5: Predictions for charged particles multiplicity distributions at LHC.

In this formulation, the model at very high energies (starting from $\sqrt{s} \sim 10$ TeV) predicts $s^\Delta/\ln^2 s$ asymptotic behavior for particles rapidity density at mid-rapidity and $s^\Delta/\ln s$ for mean number of secondary particles in the full phase-space. We stress that the contribution of enhanced diagrams (the interaction between Pomerons) that we do not take into account here are expected to be essential at these energies. With the account of these diagrams $(dN/dy)_{y=0} \sim \ln^2 s$ and $\langle N \rangle \sim \ln^3 s$ asymptotic behaviors are expected. MC

realization of the model with account of enhanced diagram is formulated in [25].

In Fig. 6 we give a description of UA5 data [26] on charged particles pseudorapidity distribution in single diffractive events at $\sqrt{s} = 900$ GeV (dissociation of one of the colliding particles is considered) and give a prediction for $\sqrt{s}=14$ TeV. For both energies the spectra are calculated by integrating over all masses of the diffractive system (up to $M^2/s \leq 0.05$). More comparisons with UA4 and UA5 data on SD events can be found in [8].

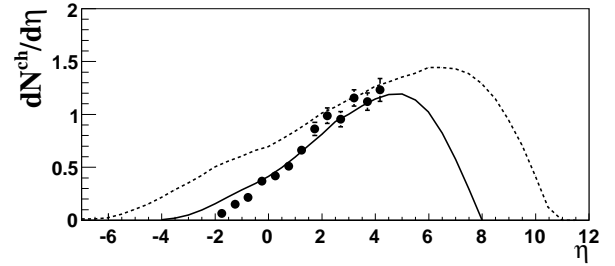


Figure 6: Charged particles pseudorapidity distributions at $\sqrt{s} = 900$ GeV (solid line) and 14 TeV (dotted line) in single diffractive dissociation events. The data points are from UA5. The indicated errors are statistical and the systematical errors are unknown.

4 Conclusion

In this paper we compare QGSM predictions with $Spp\bar{S}$ and Tevatron data on charged particles pseudorapidity and multiplicity distributions and give predictions for LHC. We stress that there are no free parameters in this analysis and hope that this approach will give a reliable predictions for particle production at LHC energies.

5 Acknowledgements

The work of A.B.K. was partially supported by the grants RFBR 0602-72041-MNTI, 0602-17012, 0802-00677a and Nsh-4961.2008.2.

References

- [1] A.B. Kaidalov, Phys.Lett. **B116** (1982) 459; Phys. Atom. Nucl. **66** (2003) 1994; Phys. Usp. **46** (2003)

- 1121; A.B. Kaidalov and K.A. Ter-Martirosyan, Sov. J. Nucl. Phys. **39** (1984) 979; **40** (1984) 135.
- [2] A. Capella, et al., Z. Phys. **C3** (1980) 329; Phys. Lett. **B114** (1982) 450; Z. Phys. **C10** (1981) 249; Phys. Rep. **236** (1994) 225.
- [3] A.B. Kaidalov, Z. Phys. **C12** (1982) 63.
- [4] P.E. Volkovitskii and A.B. Kaidalov, Sov. J. Nucl. Phys. textbf35 (1982) 720, 909.
- [5] A.B. Kaidalov, JETP Lett. **B32** (1980) 474.
- [6] G.H. Arakelian, et al., Eur. Phys. J. **C26** (2002) 81.
- [7] A.B. Kaidalov and O.I. Piskunova, Sov. J. Nucl. Phys. **41** (1985) 816; Z. Phys. **C30** (1986) 145.
- [8] A.B. Kaidalov and M.G. Poghosyan, *submitted to EPJ C*, arXiv:0910.1558 [hep-ph].
- [9] K.A. Ter-Martirosyan, Pisma Zh.Eksp.Teor.Fiz.15 (1972) 734.
- [10] K.A. Ter-Martirosyan , Sov. J. Nucl. Phys. 44 (1986) 817.
- [11] A.B. Kaidalov, Pisma Zh. Eksp. Teor. Fiz. 32 (1980) 494.
- [12] N. Armesto, et al., Z.Phys. C73 (1997) 309-313.
- [13] A.B. Kaidalov, Sov. J. Nucl. Phys. 45 (1987) 902.
- [14] A.B. Kaidalov and M.G. Poghosyan, in Proceedings of the 13th International Conference On Elastic and Diffractive Scattering (blois Workshop) 09 (to be published). arXiv:0909.5156 [hep-ph].
- [15] Albajar et al. Nucl. Phys. B335 (1990) 261; D. E. Acosta et al. Phys. Rev. D65 (2002) 072005.
- [16] T. Aaltonen et al., arXiv:hep-ex/0904.1098.
- [17] G.J. Alner et al., Z.Phys. C33 (1986) 1; Phys. Rep. 154 (1987) 247.
- [18] F. Abe et al., Phys. Rev. D41 (1990) 2330; R. Harr et al., Phys. Lett. B401 (1997) 176.
- [19] C. Albajar et al., Nucl. Phys. B335 (1990) 261.
- [20] K. Aamodt et al., JINST 0803 (2008) S08002.
- [21] G. Aad et al., arXiv:0901.0512 [hep-ex]; G.L. Bayatian et al. J.Phys. G34 (2007) 995.
- [22] Z. Koba, H.B. Nielsen and P. Olesen, Nucl. Phys. B40 (1972) 317.
- [23] A.B. Kaidalov and K.A. Ter-Martirosyan, Phys. Lett. B117 (1982) 247.
- [24] R.E. Ansorge et al., Z. Phys. C43 (1989) 357. G.J. Alner et al., Phys. Lett. B160 (1985) 193.
- [25] S. Ostapchenko, Nucl. Phys. Proc. Suppl. B151 (2006) 143.
- [26] R.E. Ansorge et al., Z. Phys. C33 (1986) 175.